Title

A Novel Wireless Health Orthopedic System Integrating Motion and Acoustic Emission Monitoring

Author

Paul, Manda

Publication Date

2013

Peer reviewed|Thesis/dissertation

UNIVERSITY OF CALIFORNIA

Los Angeles

A Novel Wireless Health Orthopedic System

Integrating Motion and Acoustic Emission Monitoring

A thesis submitted in partial satisfaction

of the requirements for the degree Master of Science

in Electrical Engineering

By

Manda Paul

2013

ABSTRACT OF THE THESIS

A Novel Wireless Health Orthopedic System

Integrating Motion and Acoustic Emission Monitoring

by

Manda Paul

Master of Science in Electrical Engineering

University of California, Los Angeles, 2013

Professor William J. Kaiser, Chair

Cost effective, wireless, wearable and robust systems are imperative for allowing us to shift our focus from the traditional event-driven healthcare model to a pervasive health awareness model where we are continuously monitoring a person's well-being. This capability will not only prove essential for timely diagnostics and early treatments, but will enable an array of tools for furthering scientific knowledge. Bringing these benefits to the orthopedic applications is of great important, since degeneration of joins is known to be a leading cause of chronic disability in the United States [1].

Monitoring acoustic emissions from joints has been previously studied to demonstrate that via quantization, clinically healthy and osteoarthritic joints can be distinguished. In the trials, piezoelectric transducers were used to detect sound waves emitted from knee joints during sit-stand-sit movements [5]. Such systems have previous been limited by the size and complexity of the acquisition unit, thus only a very limited range of activities have been monitored.

In this thesis, we present the novel Wireless Health Orthopedics (WHO) system, the developed hardware, as well as the accompanying software architecture. The specifics of the acoustic emissions (AE) system are shown in detail. We then explain how it interacts with the joint angle monitoring (JAM) measurements. We discuss the implementation of the holistic WHO system in healthy subject trials, which include sit-stand-sit, leg-extensions, walking and climbing stairs as movement sets. We further describe data post processing algorithms and techniques for synchronizing and visualizing the acquired measurements. Preliminary results indicate a quantitative difference between healthy young knee joints and healthy older knee joints. Further analysis allows for the discovery of distinct wave characteristics unique to certain movements and certain participant profiles. Finally, synchronized and superimposed acoustic emission and joint angle monitoring data is presented.

The thesis of Manda Paul is approved.

Chi On Chui

Majid Sarrafzadeh

William J. Kaiser, Committee Chair

University of California, Los Angeles

2013

Table of Contents

List of Figures

Acknowledgements

First, I would like to express my sincerest gratitude to my advisor, Professor William J. Kaiser; for his timeless patient, tireless guidance, and priceless mentorship.

I would like to thank the members of my thesis committee, Professor Majid Sarrafzadeh and Professor Chi On Chui for their invaluable help and feedback with my thesis.

I would like to thank Henrik Borgstrom for his encouraging leadership, Digvijay Singh and Vincent Zegarski for their diligent assistance in hardware design, and Celia Xu for her unmatched support of motion tracking and signal processing. I would like to further thank all my fellow colleagues and dear friends at the Wireless Health Institute and ASCENT among whom I feel like family!

Finally, I would like to dedicate this thesis to my parents and my brother for everything they have sacrificed for me so I may follow my dreams.

Chapter 1

Introduction

Arthritis is the leading cause of chronic disability in the United States. An estimated 50 million U.S. adults live with arthritis from which about 21 million have limited activities. Although arthritis is more common among adults aged 65 years or older, people of all ages can be affected. Nearly two-thirds of people with arthritis are younger than age 65 years. It is estimated that each year, arthritis results in 992'100 hospitalizations and 44 million outpatient visits [1]. The total cost of arthritis, including direct medical costs and indirect costs from lost earnings, is approximated to be hundreds of billions of dollars each year. For the arthritic patients, early diagnosis, effective pain management and treatment are of utmost importance [2].

Osteoarthritis is a degenerative joint disease which has symptoms of joint pain, tenderness, stiffness and locking. When the cartilage protecting the bones wears off, the bones become exposed and damaged. Osteoarthritis (OA) commonly affects large weight bearing joints such at the knees and hips. Knee OA is characterized clinically by usage-related pain and functional limitation. Risk factors that are strongly associated with the incidence of knee OA include increasing age over 50 years, female gender, higher body mass index, previous knee injury, recreational usage, and family history. Radiography is often used as the 'gold standard' for morphological assessment of knee OA. The most classical feature noticed is the narrowed joint spacing. Although rare, further imaging modalities such as magnetic resonance imaging, ultrasound and scintigrphy can be used for diagnosis. Imaging can provide high resolution views

of an OA knee, however, it is incapable of offering information about the integrity of the knee joint in motion [3]. The inconvenience, prolonged preparation, and cost of the system render imaging modalities useless in analyzing the dynamic health of the knee. It is apparent that methods are needed for diagnostics of human joints which will not harm the patient by radiation or by invasive examinations. We will look deeper at a different approach for assessing and monitoring the knee joint in motion [4].

Previously, piezoelectric transducers have been used to detect sound waves emitted during knee movements [5]. To develop protocols for data collection and analysis, acoustic emissions (AE) from volunteers with clinically healthy knees and patients with radiologically confirmed knee osteoarthritis have been studied. The trials included sets of sit-stand-sit movements. It has been demonstrated that quantification of acoustic emissions can distinguish between clinically healthy and OA knees [6, 7]. Previous systems have been limited by the size and complexity of their acquisition unit, thus only a very limited range of activities has been monitored.

The objective of this thesis is to demonstrate a novel wireless health orthopedic system, integrating both motion and acoustic emission detections. This high rate system would allow physicians to monitor the patients' knee health and diagnose based on acoustic emissions during various activities such as sit-stand-sit, walking and climbing stairs. The Wireless Health Orthopedic (WHO) system is described as a platform for monitoring joint health. This thesis will focus on the design and implementation of the system for the knee, followed by results of the healthy subject trials.

Chapter 2

System Design

In this chapter the WHO system design is presented. For each of the two major portions, acoustic emission (AE) sensing and joint angle motion (JAM) monitoring, both the hardware and software used is described in detail.

2.1 System Overview

The WHO system enables the simultaneous monitoring of knee joint acoustic emissions and knee joint angles. Figure 2.1 shows the overall block diagram of the entire system. Data is collected from the AE Sensor and the Motion Sensor via cRIO and MotionFit Board respectively. Then the data is transmitted to a host unit where the data is stored and processed. Data processing and visualization is done in MATLAB.

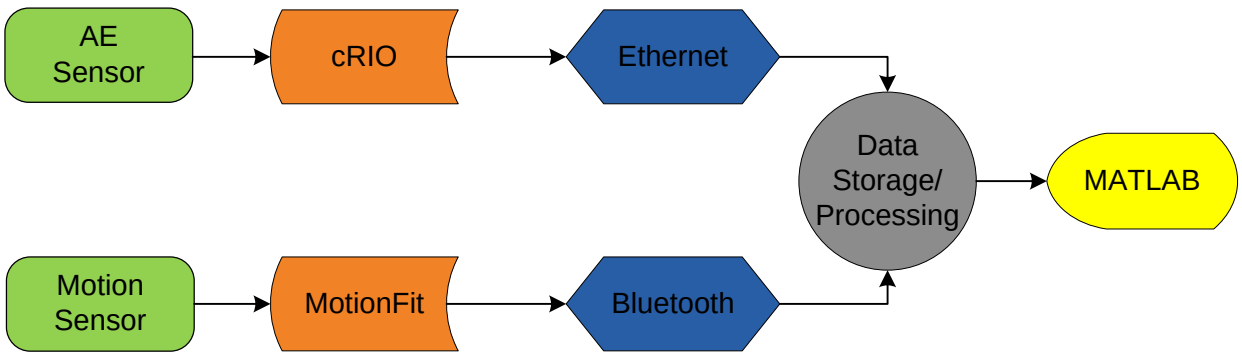

Figure 2.1: Block Diagram of AE System

The following section provides an in-depth description of all of the components encompassing

the hardware and software. Figure 2.2 shows the interconnections of the system components.

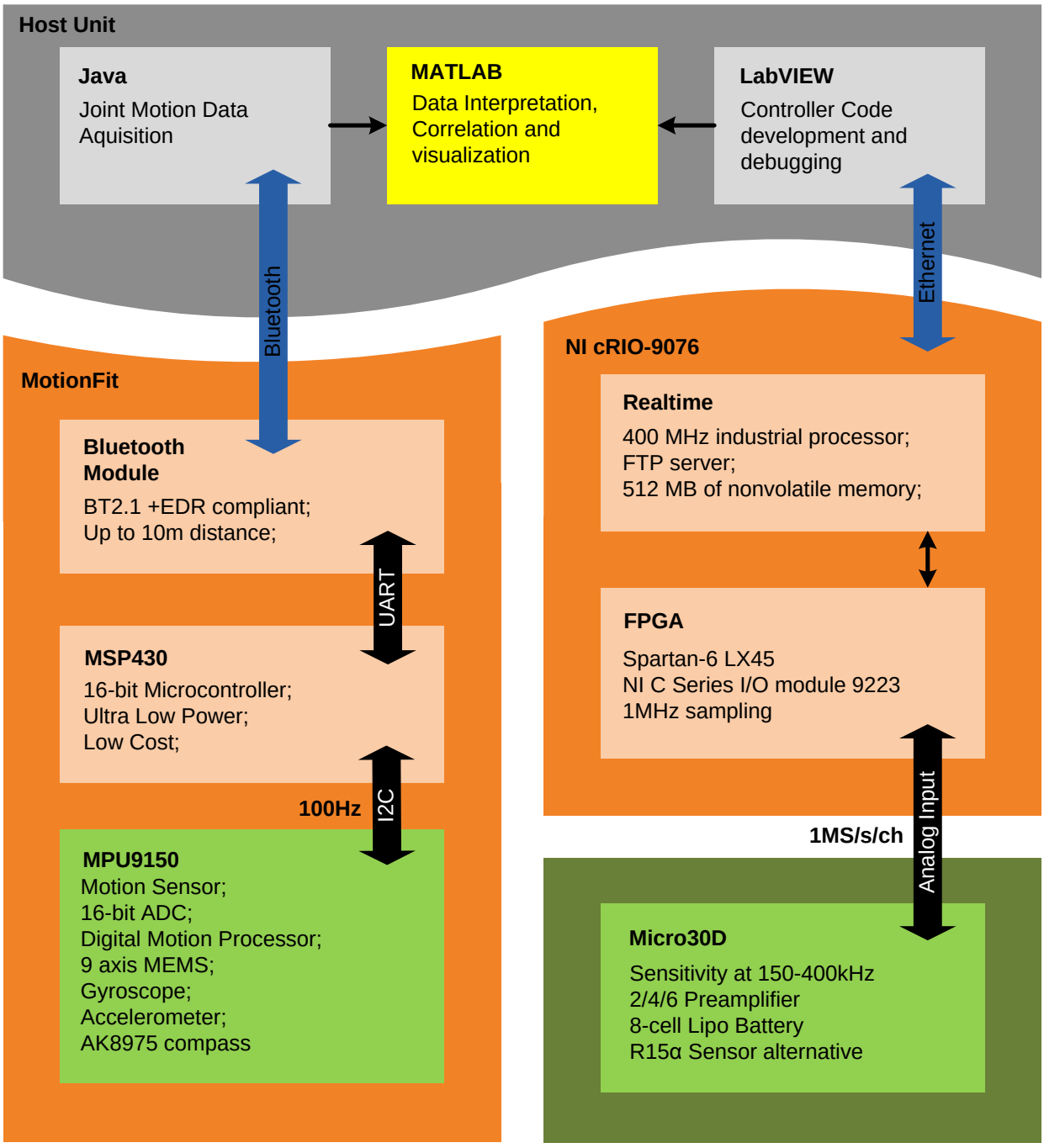

Figure 2.2: Interconnections of AE System

2.2 Acoustic Emission (AE)

The system development specifics of the acoustic emissions portion are discussed. This is summarized by the right sides of figure 2.2.

2.2.1 Hardware

We will first take a look at the data acquisition hardware, then move to the details of the sensor system.

2.2.1.1 Data Acquisition

The AE system implementation is designed to provide high data rate sampling and robustness. For this purpose we have utilized the performance capabilities of the NI cRIO-9076 shows in figure 2.3a. The CompactRIO integrated system combines an industrial real-time controller and reconfigurable field-programmable gate array (FPGA) for monitoring applications. It contains a 400 MHz real-time processor with an embedded reconfigurable Spartan-6 LX45 FPGA chip.

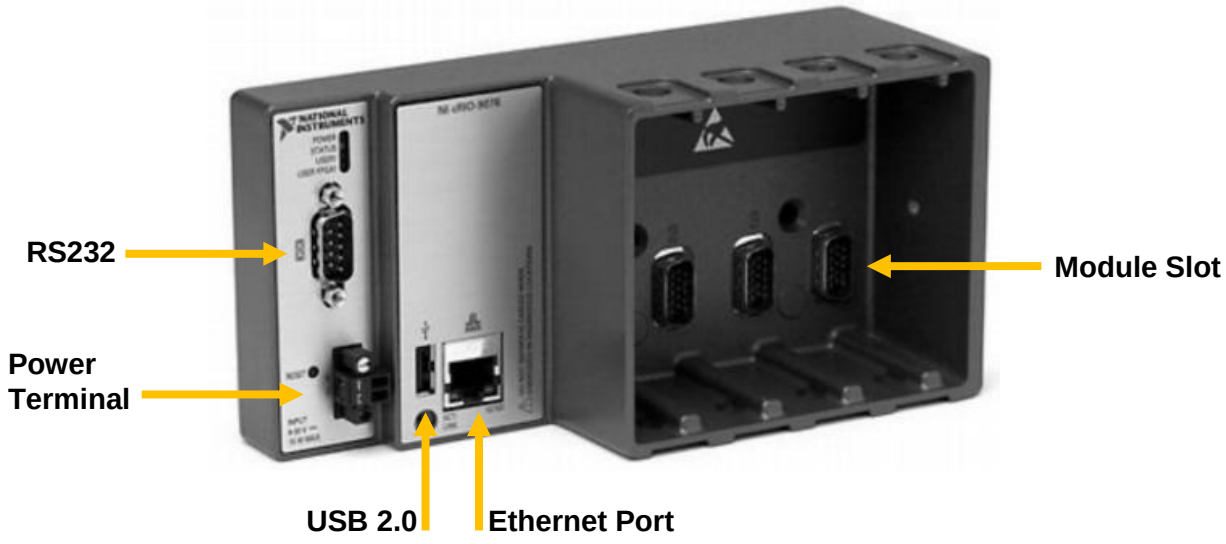

Figure 2.3a: NI cRIO-9076

The Ethernet port allows for programmatic communication over the network to a host PC or enterprise system. This new cRIO also features a USB 2.0 port for data storage and connection to peripheral devices. In terms of network features, the cRIO has the ability to be synchronized with an SNTP time server. Although cRIO-9076 lacks a backup battery for the Real-Time Clock, this is not a setback for our design. The compensation for this feature and the power source will be discussed at later sections. Specifications for the cRIO-9076 are listed below [8].

- Embedded real-time controller
- 2M gate reconfigurable FPGA chassis (Spartan-6 LX45)
- 400MHz real-time processor
- Voltage: 9-30V
- Interfaces: Ethernet, USB 2.0, RS232
- Network: Build-in FTP/HTTP servers
- Memory: 256MB DRAM, 512MB nonvolatile storage
- Active Current Consumption (AE application): 200 mA
- Physical Specifications: 7.01 x 3.47 x 2.31 inches (17.81 x 8.81 x 5.89 cm)
- Weight: 22.68 oz (643 grams)

The cRIO-9076 accepts 4 NI C Series I/O modules, which are plugged into the module slots on the chassis. The FPGA circuitry in the chassis controls each I/O module and passes data to the controller though the local PCI bus. A wide variety of modules are available from which we have made use of NI-9223 shown in figure 2.3b. This module is a high-speed, simultaneous module for use in any of the NI Compact chassis including the cRIO-9076. It uses four 16-bit analog-to-digital converters for true simultaneous sampling at up to 1MS/s per channel. An added

advantage is that all analog input modules installed in the same chassis can be synchronized to share the same sample clock.

Figure 2.3b: NI 9223

Specifications for the cRIO-9076 are listed below [9].

- 1MS/s/ch sampling rate
- 16-bit ADC resolution
- ±10.6 V range
- Physical Specifications: 0.900 x 3.469 x 2.776 inches (2.29 x 8.81 x 7.05 cm)
- Weight: 4.9 oz (138 g)

Communication between the cRIO and the Host Unit (Dell laptop), as seen in figure 2.2, are accomplished through an Ethernet connection. This takes advantage of the cRIO's built in FTP server. To make this connection wireless, we have employed the use of the Ethernet Bridge in figure 2.4. The bridge communicates with the wireless chip on the Host Unit and seamlessly replaces the Ethernet cable. WET54G weighs 8.50 oz (240 g) and is 4.96" x 1.06" x 4.21" (126 x 27 x 107 mm) [10].

Figure 2.4: Wireless Ethernet Bridge (WET54G)

2.2.1.2 AE Sensor System

Looking at figure 2.2 it can be seen that the NI module 9223 is connected to the AE sensor system via its analog input. In this section we will discuss the details of this connection and the specifics of what the AE sensor system entails. There are two AE sensors that we have looked to employ in our system. The first of which is the R15α Sensor from MISTRAS Group shown in figure 2.5.

Figure 2.5: R15α Sensor

The R15α is a narrow band resonant sensor with high sensitivity. The sensor cavity is machined from a solid stainless steel rod, making the sensor extremely rugged and reliable. The ceramic face along with a 30 degree chamfer to cavity electrically isolates the sensor cavity from the structure under test assuring a low noise operation. The compact size of the sensor makes it readily suitable for deploying in tight spaces for monitoring. This general purpose sensor

provides a good combination of high sensitivity and low-frequency rejection and is designed for monitoring common structures such as bridges, pipelines and vessels in mind. However, this does not deter us from using its features to our benefit in this application. Specifications for the R15α are listed below [11].

- Peak Sensitivity, Ref V/(m/s): 80 dB
- Operating Frequency Range: 50-400 kHz
- Resonant Frequency, Ref V/(m/s/): 75 kHz
- Shock Limit: 500 g
- Physical Specifications: 0.75 diameter x 0.88 inches height (1.9 x 2.24 cm)

The pre-amplifier used with the R15α is the 2/4/6 Preamplifier from Physical Acoustics Corporation shown in figure 2.6.

Figure 2.6: 2/4/6 Preamplifier

The 2/4/6 Preamplifier is designed to be used with all available AE systems that have their power supplied via their output signal BNC cables. Provided with 20/40/60 dB switch selectable gain, this preamplifier operates with either a single-ended or differential sensor. Plug-in filters provide the flexibility to optimize sensor selectivity and noise rejection. These filters are supplied in the

different filter configurations, and offer constant insertion loss for easy filter swapping without the need for recalibration. Specifications for the 2/4/6 preamplifier are listed below [12].

- Wide dynamic range < 90dB standard
- Low noise <2 microvolts (with standard filter and input shorted)
- Large output signal - 20Vpp into 50 ohms
- Single power/signal BNC or optional separate power/signal BNC
- Plug-in filters
- 20/40/60 selectable gain
- High input impedance

The second sensor that we have considered for our AE system is the Micro30D shown in figure 2.7. By contrast, it is a differential sensor designed to isolate the sensing terminals electrically from the cavity. This electrical isolation makes the sensor particularly useful for applications where high background electrical noise is a major concern. Similar to the R15α, it has a very good sensitivity and frequency response over the range of 150 - 400 kHz. The two signal leads from the sensing element feed into a differential pre-amplifier which eliminates common-mode noise resulting in a lower noise output from the pre-amplifier. This sensor features a rugged steel construction and a dual BNC connector with an integrated twin axial cable exiting on the side. Although smaller in size, its capabilities do not dim compared to the R15α sensor. The Micro30D is well suited for structural health monitoring of large structures like storage tanks. Our application requires a high fidelity AE response which can be provided by this wideband sensor. Specifications for the Micro30D preamplifier are listed below [13].

- Peak Sensitivity, Ref V/(m/s): 65 dB

- Operating Frequency Range: 150-400 kHz
- Resonant Frequency, Ref V/(m/s/): 125 kHz
- Shock Limit: 500 g
- Physical Specifications: 0.7 diameter x 0.65 inches height (1.78 x 1.65 cm)

Figure 2.7: Micro30D Sensor

The sensitivity of the sensor is high enough such that small touches to the sides and the back of the sensor causes signals that are comparable to the AE signals we are interested in. It becomes imperative for the sensor to be placed in a housing. Figure 2.8 shows a clamp fastened snug around the sensor. This alleviates some of the signals that would otherwise be captured as false AE events. The same type of clamp can be made for the R15α sensor. The clamp also prevents the sensor from tilting onto its side when it is inside the knee brace. Its usage is thoroughly explained in the Healthy Subject Trials chapter.

Figure 2.8: Micro30D Sensor Housing

The pre-amplifier used with the Micro30D is the IL60D Preamplifier from Physical Acoustics Corporation shown in figure 2.9. Similar to the 2/4/6 preamplifier described earlier, IL60D was also designed to be used with AE systems that have their power supplied via their output signal BNC cables. This low noise preamplifier has fixed gain and fixed filter bandwidths. Its small and compact size, along with its fixed specifications, allows this preamplifier to be a more cost effective solution. From the different available models, we have chosen the 60 dB gain amplification. It also has an active filter built in and optimized sensor selectivity and noise rejection. Similar to the 2/4/6 preamplifier, the operating range of IL60D is 18-28V [13].

Figure 2.9: IL60D Preamplifier and filter

2.2.1.3 Power Source

The operating range of the cRIO is 9-30V, where as the preamplifiers require a minimum of 24V). To accommodate both, we have made use of TP3300-8SPP25 Lithium Polymer batteries from Thunder Power RC shown in figure 2.10. LiPo batteries are rechargeable batteries composed of identical secondary cells to increase the discharge current capability. They have gained popularity in the world of radio-controlled aircrafts and cars, largely because of their low weight and great power delivery. These qualities make them a great choice for our application, and are preferred over nickel-metal hydride batteries. As its name suggests, the TP3300-8SPP25

is a 3300mAh 8-Cell battery that has an operating voltage at 29.6V. Our choice of the type is determined by the length of our perceived healthy and patient trials before a recharge is needed. Also it was important for us to be able to comfortably power both the cRIO and the preamplifier with the same source. Using two 24 volt regulators we accomplish just that.

Figure 2.10: TP3300-8SPP25 Lithium Polymer

Figure 2.11: TP1430C charger

The 8-cell LiPo comes in at about 21.6 ounces (611 grams) and has dimensions of 2.0 x 1.7 x 5.3 inches (5.0 x 4.3 x 13.5 cm). Figure 2.11 shows the charger appropriate for the LiPo batteries. The TP1430C has a built-in cell balancer and a charge rage of up to 30Amps for ultra-fast charging [14]. The overall system is connected to fit inside a small case. Figure 2.12, is an

iteration of the setup which shows the contents of the pack. Figure 2.13 shows the pack containing the entire AE system along with the wireless Ethernet bridge. The wearable version will be featured in the Healthy subject trials chapter.

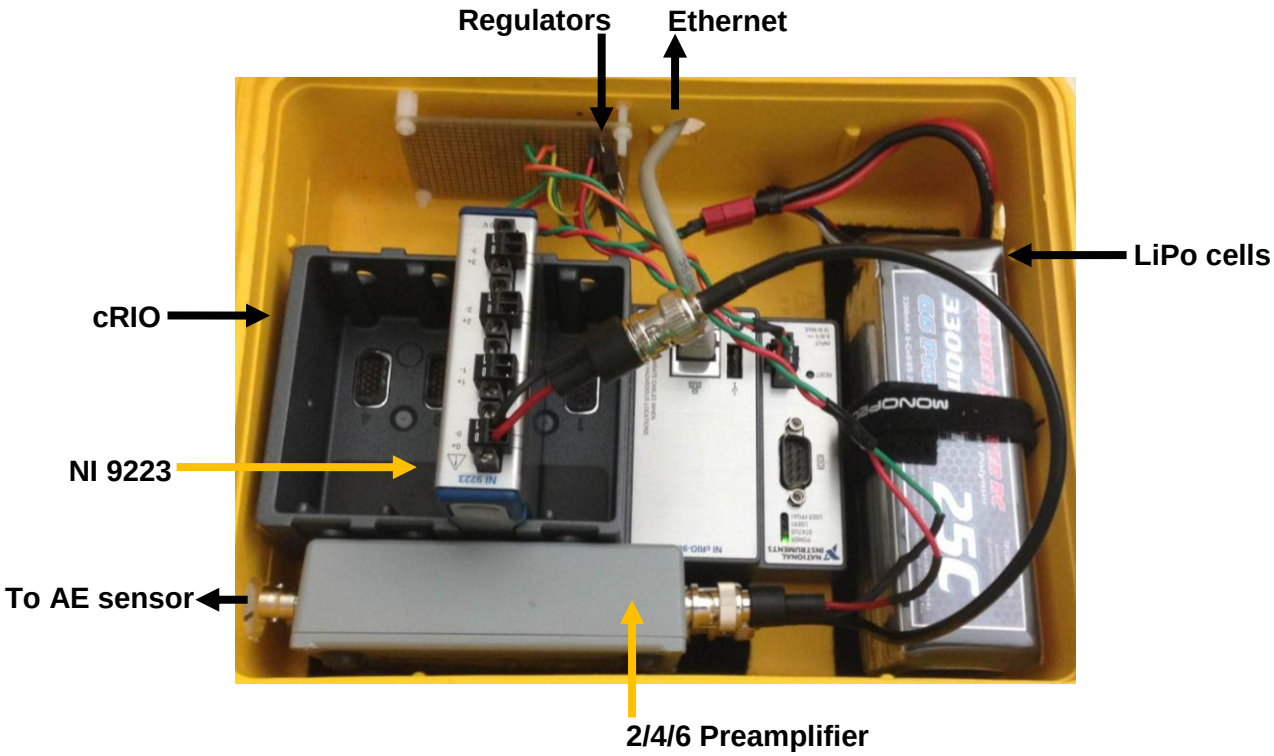

Figure 2.12: Overall AE hardware

Figure 2.13: Wearable wireless pack

2.2.2 Software

The AE system software is created in LabVIEW. The FPGA and Host Unit (HU) code development for the cRIO is presented here. LabVIEW allows for the synchronization of embedded code execution to an FPGA-generated interrupt requests or an internal millisecond real-time clock source. The real-time OS simplifies the development of our application which includes acquisition loops, post processing, data logging and Ethernet communication. We make use of the built in elemental I/O function such as FPGA Read/Write functions which provide a communication interface to the highly optimized reconfigurable FPGA circuitry. Via the controller, the Host code reads, processes and saves the appropriate code.

2.2.2.1 FPGA Code

The FPGA code development process is shown in figure 2.14. The FPGA VI is first created in a designated project in LabVIEW. Then, after iterations of emulation and testing, the VI is converted to VHDL. The Xilinx compiler then generates a corresponding bit-stream file and become ready to be deployed onto the FPGA.

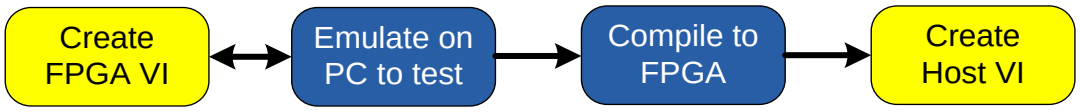

Figure 2.14: FPGA code development process

A very simple code snippet can be seen in figure 2.15. Although graphical programming might seem odd, it does provide a much faster turnaround for prototyping our application. Here four channels of analog input are sampled simultaneously and combined into an array. The array is

passed into a For Loop which then indexes through each element and passes it through to a digital memory access (DMA) FIFO [15].

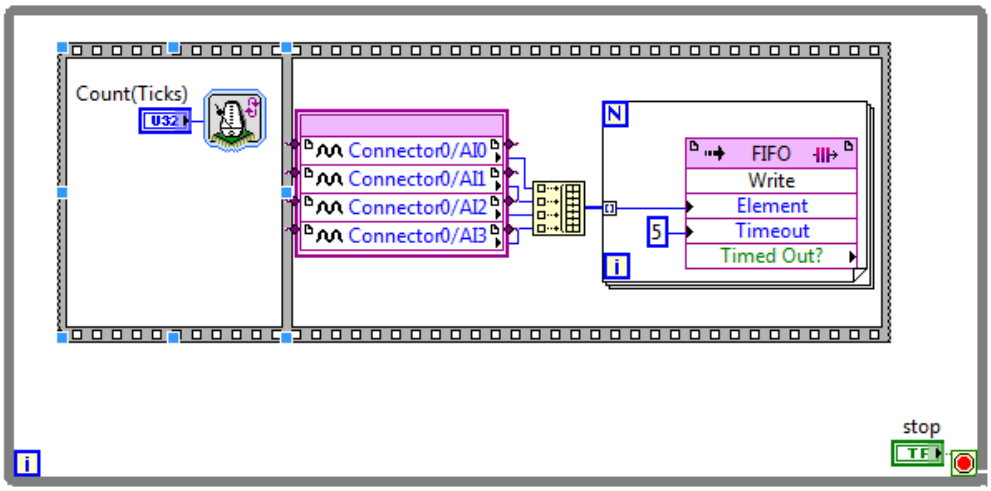

Figure 2.15: FPGA Code Snippet

2.2.2.2 Host Code

On the host side a code can be developed to access the DMA FIFOS and methods. Figure 2.16 shows such a code snippet. The Open FPGA VI References function is called which the Invoke Method Node uses to allow access to the FIFOs. After configuration and the start method a loop is entered in which data can be read. Once the stop button is pressed the loop exists and the Stop method is called to free all allocated resources [15].

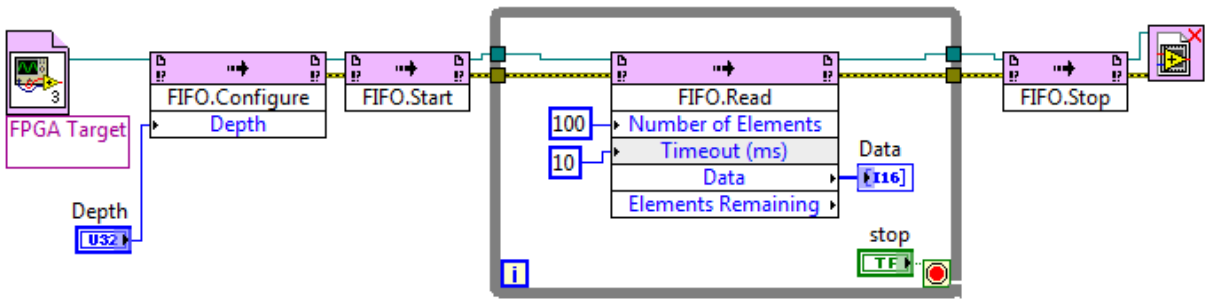

Figure 2.16: Host Code Snippet

Many interesting procedures can be done in the VI on the Host Unit. For our application, the main loop looks very similar to figure 2.16 in structure. A few more functionalities are in as needed. We have setup up a write loop to run in parallel, in which the read data is being organized and written into a file from which we can extract the individual events of interest. The main loop not only has the responsibility of collecting the data, but it also does event triggering. As a buffer is read, the standard deviation is calculated and compared against a threshold determined by the user. If that buffer contains an event of interest, it is saved along with the data before and after that particular event. Although there is an optimum buffer size, it can be changed based on end user specifications. A larger buffer would retain a much larger set of data points for each event, however, based on the characteristics of the events we are expecting in our application, a size of 4000 is found to be appropriate. Once this buffer is obtained, there are a number of operations that can be done to determine if the data is a significant event or if it can be discarded. Wave features such as peak-to-average ratio, maximum amplitude, and variance are some characteristic parameters with which we can distinguish between AE events and signals from other sources. We have implemented variance as our main threshold. The actual value is determined empirically and is found to be 0.006. We can also sift through the data further by putting on more restrictions during post processing. For this to work in a meaningful manner, the data needs to be organized precisely. This is when time synchronization comes into play. The cRIO has the capability to connect to a network time protocol (NTP) server for its time calibration. We have set up a server on the Host Unit, which is the personal computer, for the cRIO to use. Figure 2.17 is a snippet of the code which time-stamps the data collected with the appropriate time. Here, it can be seen that there are two files being saved for each trial. One contains the data of the acoustic waveforms from the joints. The other contains the time-stamps

of all the events. At a later section we will discuss the time-stamped data from the JaM portion and how these two are used for overall data synchronization.

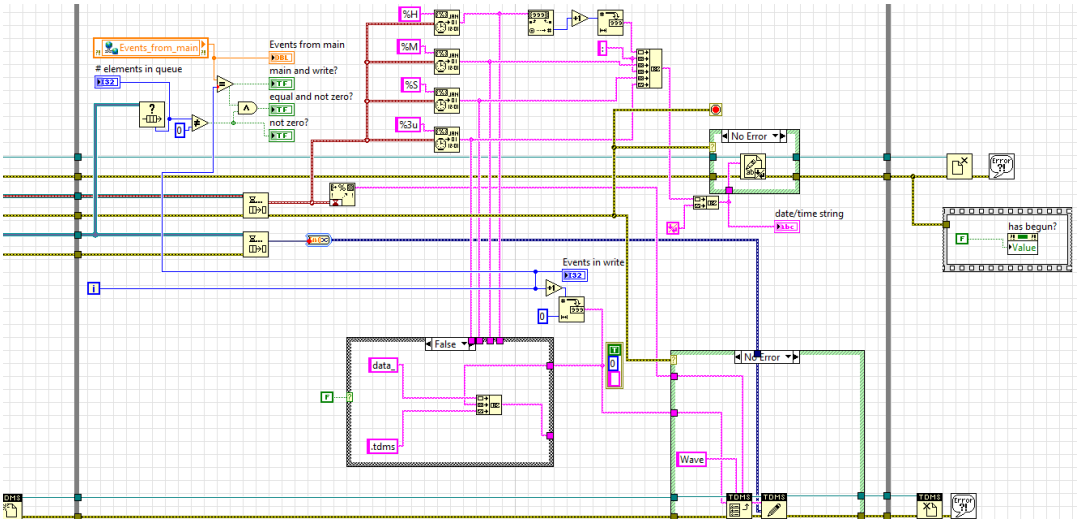

Figure 2.17: time synchronization and data saving

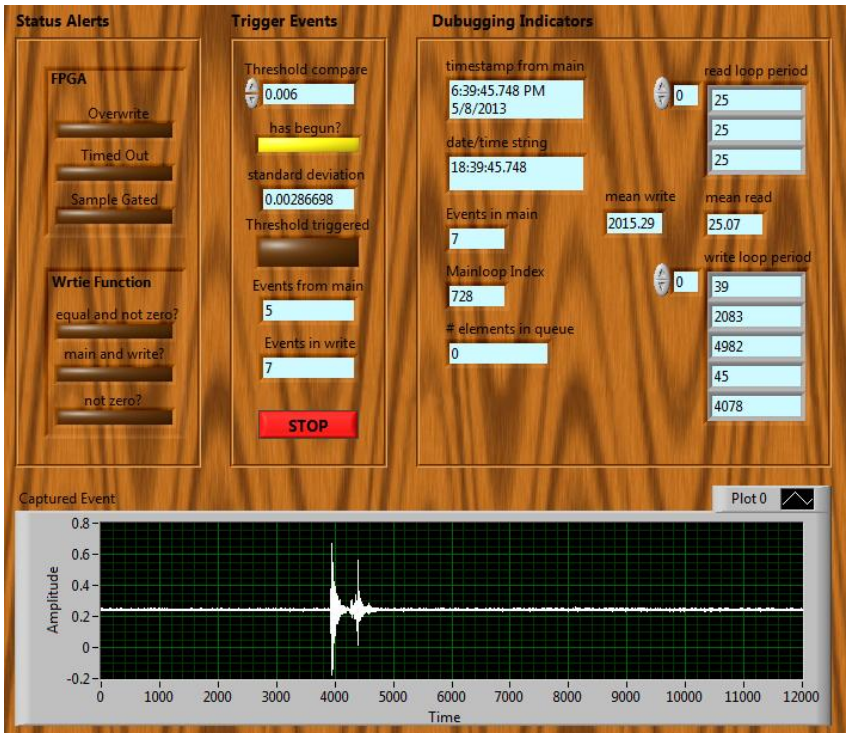

Figure 2.18: Graphical user interface for Host Unit code

An important part of the software for the AE portion is the graphical user interface which is on the Host Unit. This is a powerful interface for controlling variable, getting immediate feedback and access to debugging. Figure 2.18 shows indicators for statuses of anything from FPGA to the specific functions used. Also, here many function variables are printed out for the user to see. The variance threshold can also be adjusted from this screen. At the bottom, the last captured waveform is shown. The captured events are shown as they occur.

2.3 Joint Angle Motion (JAM)

The system development specifics of the joint angle motion portion are discussed. This is summarized by the left sides of figure 2.2.

2.3.1 Hardware

The entirety of the joint angle motion hardware can be boiled down to the MotionFit board from InvenSense in figure 2.19. This Wireless solution is meant for rapid commercialization of wearable sensors for fitness, health and sports applications. Specifications for the MotionFit are listed below. The MPU-9150 is emphasized, since that chip presents an utter importance to our application.

- Processor: MSP 430 microcontroller
- Radio Module: BT2.1 + EDR complaint (low power: 50mA active)
- Power source: 110mAh rechargeable battery. 4 hours of streaming time.

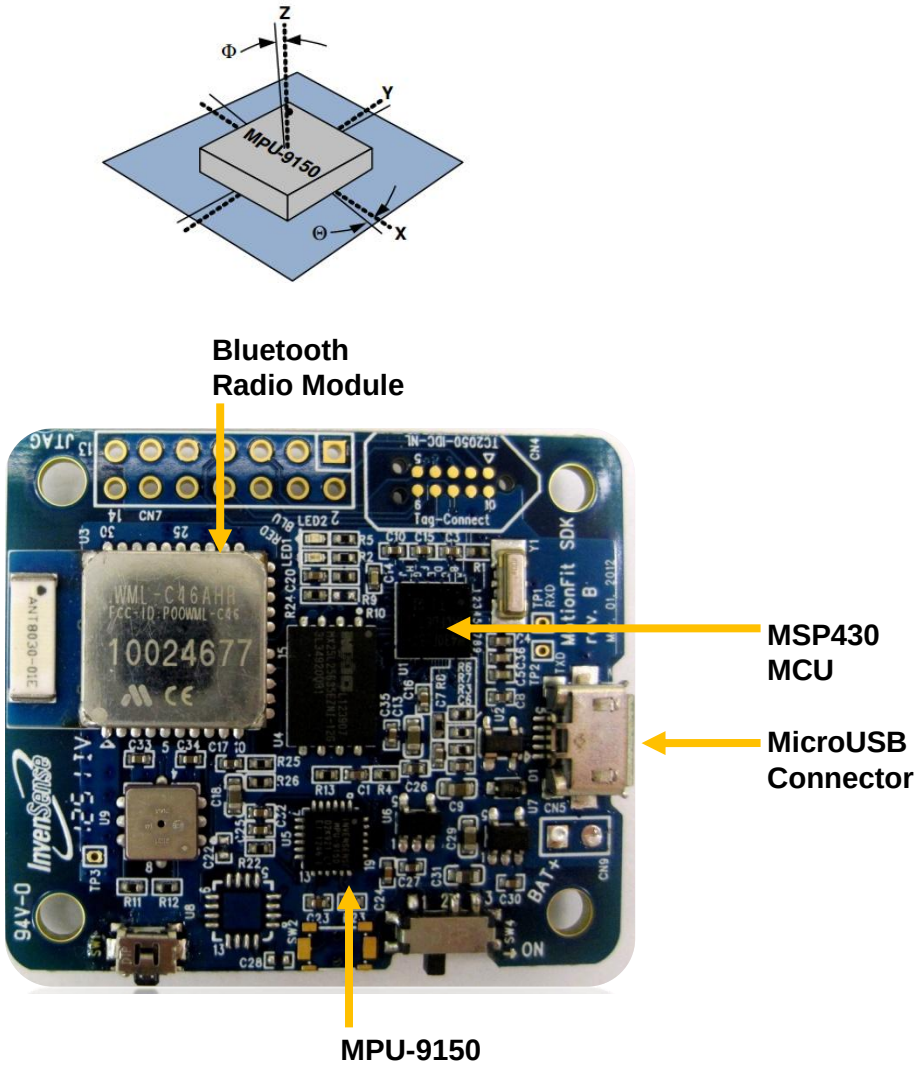

Figure 2.19: MotionFit Board

- Sensor: MPU-9150
    - Triple-axis MEMS gyroscope, accelerometer, magnetometer
    - 1024 byte FIFO
    - User-programmable digital filters
    - 400kHz fast mode I^2C communication
    - Internal Digital Motion Processing

The MPU-9150 is a 9-axis MotionTracking device designed for low power, low cost, and high performance. It consists of a run-time calibration firmware and sensor fusion algorithms for optimal delivery precision. The MPU-9150 is essentially the combination of the older MPU-6050 chip and the AK8975 3-axis digital compass. The 9-axis Motion Fusion algorithms incorporate the compass data with the 3-axis gyroscope and 3-axis accelerometer raw data. As seen in Figure m, the +Y direction is pointed towards the MicroUSB connector on the MotionFit board. The +X direction is pointed away from the Bluetooth module and is in the same plane. The +Z direction is pointed out of the board and out of the page. After the on board digital motion processing, the data is available to the user via I2C. The MSP430 microcontroller unit communicates with the MPU-9150 chip via I^2C. The MCU is also in communication with the Bluetooth module [16]. Overall we are making use of the radio to transmit the gathered and modified data to the Host Unit, which in the current iteration of the AE system, is a Dell laptop.

2.3.2 Software

The JaM system software is in two parts. The first are the firmware that is uploaded onto the MotionFit sensor, and the script that is ran on the Host Unit. The second are the MATLAB code and algorithms which are used for sensor verification and data post processing.

2.3.2.1 MotionFit Code

We will first present the the MotionFit firmware overview shown in Figure 2.20. When the board has first been turned on, it initializes the microcontroller, then initializes the sensors and enters the calibration state.

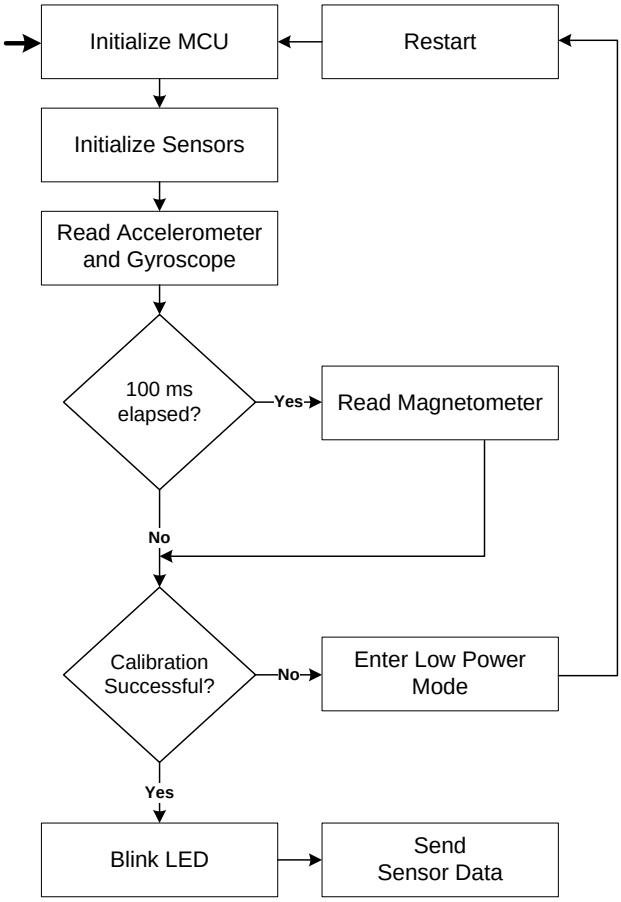

Figure 2.20: Firmware overview

Any major changes to the accelerometer, gyroscope or magnetometer (optional), will corrupt the needed calibration data and will render the process and proceeding data useless. Upon failure the sensor enters a low power mode and needs to be restarted for continuation. On the other hand, if the on board calibration is successful, MotionFit will begin sending data to the Host Unit via Bluetooth [17]. The Host Unit is equipped with a Bluetooth dongle which can be accessed through a COM port on the Dell laptop. The Host Unit is prepared for data collection by running a script written in Java. The data is received, parsed and saved according to required protocols.

2.3.2.2 MATLAB Code

Once the data is saved, post processing in MATLAB can begin. Here, we will briefly mention the mechanics of what we are measuring. Then we will describe how the received data can be turned into meaningful join angles. Figure 2.21a) shows the placement and orientation of the Motionfit sensors on the leg. Figure 2.21b) shows a side view of the leg. The dashed line indicates the conventional placement of the sensor, which is to be on the other (medial) side of the leg.

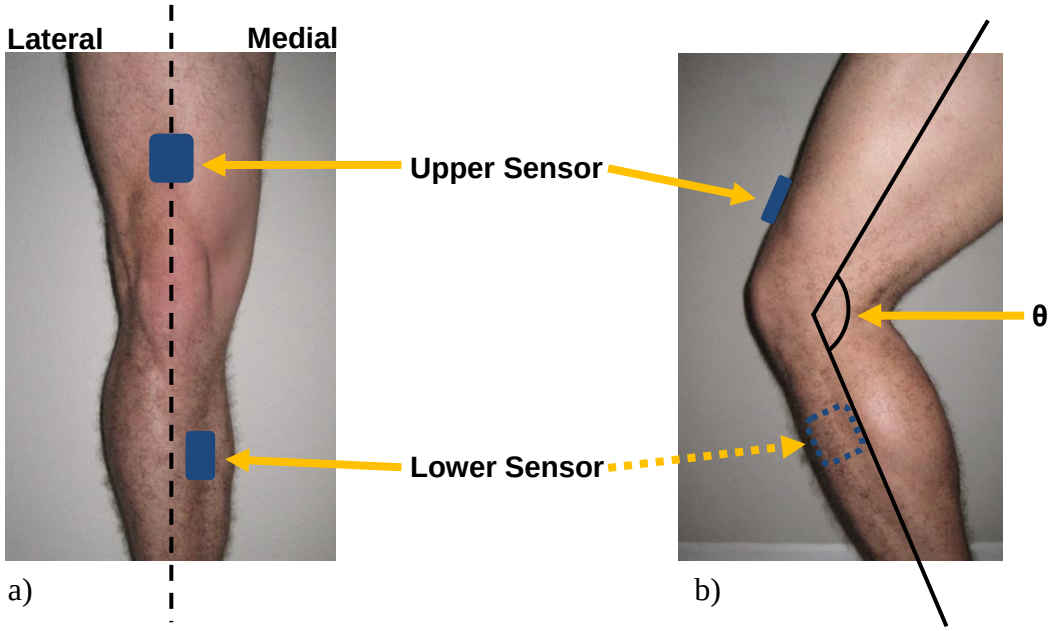

Figure 2.21: Orientation and placement of sensors

The firmware is written such that the information sent over Bluetooth contains measurements from the acceleration and the gyroscope. The reliability of the magnetometer was found to not be sufficient. As previously mentioned, MPU-9150 on the MotionFit board contains an internal Digital Motion Processing capability. This outputs quaternion values whose usage we will explain shortly. The last piece of data we add to the Bluetooth packets is an index. This helps

with confirming the order and presence of all the packets. Once the desired data is received at the Host Unit, they are time-stamped with the laptop time. Figure 2.22, shows sample data of what is saved on the Host Unit during each data collection trial.

```
1  Receiver time, Accel X,Y,Z, Gyro X,Y,Z, Quaternion W,X,Y,Z, dt(or)index
2  1368566667986,886,448,15868,-1,-2,0,1072769784,-23768410,29407234,-25627562,19203
3  1368566668007,882,406,15800,-1,-2,0,1072769742,-23767289,29409458,-25627786,19204
4  1368566668027,854,412,15786,-1,-1,0,1072769905,-23767299,29403223,-25628104,19205
```

Figure 2.22: Sample joint angle monitoring data

To practically describe the joint angle motion from the received data, we need to obtain Euler angles, since they are easier to visualize and grasp conceptually. The MPU-9150 DMP outputs quaternion because they are a more convenient mathematical notion for representing orientation and rotation of objects in three dimensions. Equation (1) is a method of converting quaternion to Euler angles.

$$\begin{bmatrix} \phi \\ \theta \\ \psi \end{bmatrix} = \begin{bmatrix} \arctan 2(2\cdot(q_0q_1+q_2q_3),1-2\cdot(q_1^2+q_2^2)) \\ \arcsin(2\cdot(q_0q_2+q_3q_1)) \\ \arctan 2(2\cdot(q_0q_3+q_1q_2),1-2\cdot(q_2^2+q_3^2)) \end{bmatrix} \quad (1)$$

The conversion can be done separately for each (upper and lower) sensor separately. The lower sensor needs a bit of more attention because it is not mounted directly on the shin, but is placed on the right side of the dashed line on the leg in figure 2.21a). To adjust for this offset, we do a calibration phase whose process will be further discussed in the Healthy Subject Trials chapter. Data synchronization between the two sensors is done by have a marker movement before the start of each trial. The marker we employ is tapping of the foot equipt with both sensors. The difference between the y-axis rotations of the sensors, along with incorporation of the offsets, gives us the joint angle motion. See figure 2.19 for orientation of y-axis on the sensor.

Chapter 3

Healthy Subject Trials

In this chapter we present the procedure for conducting healthy subject trials. We will discuss the obtained results and show the processed data.

3.1 Methods

This section will describe the study participants of the healthy trials and the testing protocols under which the trials were conducted. The methods explained here are developed for healthy subject trials. Where appropriate, modifications are suggested for patient trials.

3.1.1 Study Participants

The work presented here is from participants that were unofficially chosen for the trials. We will refer to this as the "in-house" trials. The data consists of knee AE (acoustic emissions) and JAM (joint angle motions) acquired from 4 participants. Based on self-completing assessment, the right knees of the 4 participants were classified as healthy knees with no previous injuries or symptoms of swelling or pain. For the purpose of acquiring preliminary results verifying the operation of the system, the participation group was kept small. The average age of the participants was 26.25. The participants were asked to perform a set of activities as the data was collected. The entire process took less than 10 minutes for each trial.

3.1.2 Testing Protocol

In this section we will present the steps required to prepare the participants and the environment for the trials. Then we will discuss the specifics of how the trials are carried out. The system hardware used has been described in the previous chapter. Here we will show how the participants will wear the device. The placement of the acoustic emission sensor has been under careful consideration. As mentioned, the goal of the monitoring is to be able to identify differences in acoustic emission characteristic for knee diagnostic purposes. Figure 3.1 is an anatomical view of the knee. When the knee moves, the Femur and Tibia grind against one another, cushioned by the articular cartilage, and the medial and lateral meniscus [18].

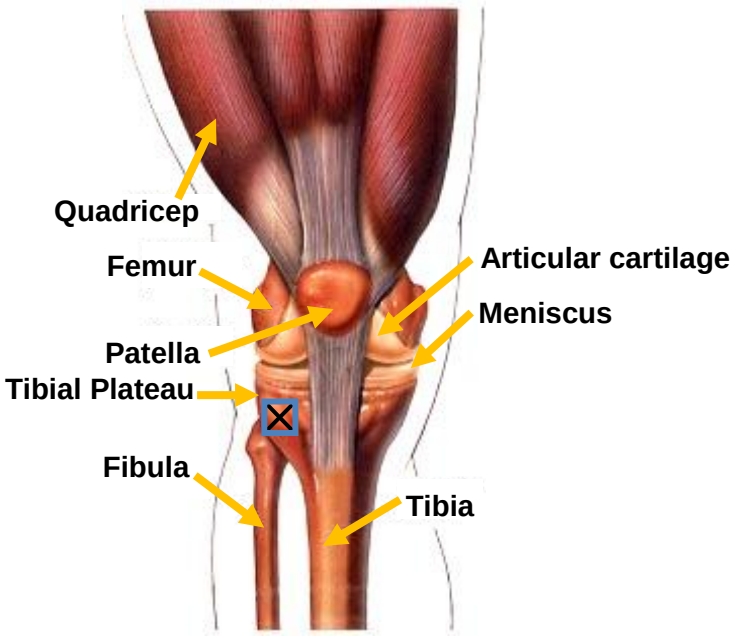

Figure 3.1: Anatomy of left knee

Knee movements generate acoustic emissions which can be detected by the piezoelectric sensor and the accompanying AE system described in the previous chapter. The AE sensor is placed on the lateral side of the knee, specifically on the tibial plateau. This specific anatomical site is

proximal to the position of contact between bone surfaces. Locating the lateral point of the tibial plateau is also quick and less complicated even if the participants are of varying size and body mass index. Furthermore, the body variations at the tibia plateau make little difference on the distance change between the sensor and the AE signals from the knee joint. Once the tibial plateau is located, the sensor is placed upon that point and the knee brace is wrapped on the knee. The elasticity of the brace allows for it to be adjusted around the sensor such that there is a consistent contact between the sensor surface and skin. Figure 3.2 shows a participant sitting on a chair to demonstrate the placement of the sensors and the knee brace.

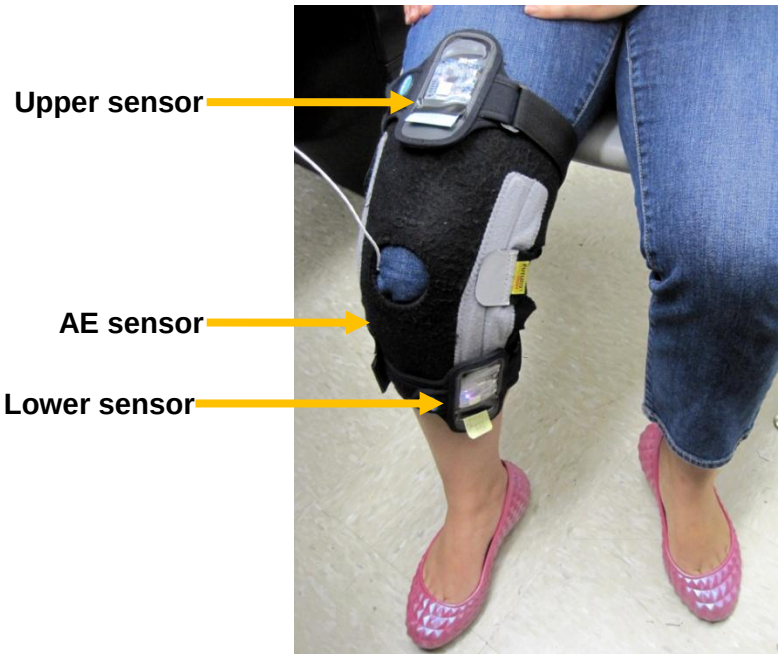

Figure 3.2: Participant pre sit-stand-sit trial

Once the sensors are placed, the MotionFit sensor needs a calibration phase. At this point the participant is asked to stand for a few seconds. Then she is asked to sit and her right leg is placed on a chair directly in front of her, such that her leg is now parallel to the ground. Once the calibration phase is over, the trial can begin. For the in-house healthy trials we have devised

three sets of motions for the participants to perform, the first of which is a set of sit-stand-sit movements. The movements consist of standing up from a normal eight chair, with no help from the arms, reaching a full standing position, and returning to a seated position. After a 15 second break, the participant stands and walks at a normal pace for about 24 feet. Then the participant walks down 6 stairs, turns around and walks back up. Figure 3.3 shows a participant ready to begin the walking set. He is wearing the sensors in a similar way to the female participant shown in the sit-stand-sit sets.

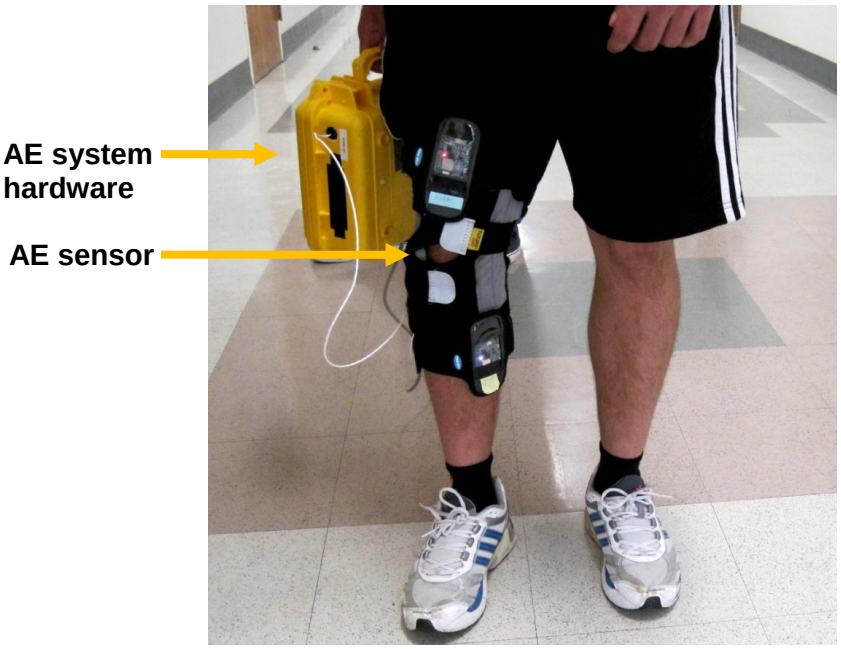

Figure 3.3: Participant during walking set

During this set, we made use of the yellow case design that can be carried in hand. As seen in the system design chapter, all the electronics for the AE system fit comfortably inside the case. The wearable version can be seen in figure 3.5. The pack is meant to be worn on the waist, and it is most comfortable on the lower back. The pack weighs less than 5 pounds and has adjustable straps to accommodate the participants. Once the walking set is done, the participant is asked to

walk to the edge of the stairs to begin the last set in the trial. Figure 3.4 is the climbing stairs set. She is asked to walk down and then up at her a comfortable pace. This concludes the trial and the sensors and the pack are removed from the participant at this time. The climbing stairs set can be eliminated from the trials if our physician does not feel the patients are capable of such an activity during our patient trials.

Figure 3.4: Participant climbing stairs

Figure 3.5: Wearable AE hardware pack

3.2 Results

The data presented here is for the purposes of demonstrating functionality of the entire system. We will discuss both the JAM and AE results. Then we will present an overlay of the two data sets and discuss the significance.

3.2.1 Joint angle Motion Results

Figures 3.6 and 3.7 are one set of data collected from a participant during sit-stand-sit movements. The red line represents the z-axis, the blue is the y-axis, and the x-axis is shown in green. There is little variation in figure 3.7, because the lower limb is somewhat stationary during a sit-stand-sit. The two valleys in figure 3.6 represent the movement of the upper leg as expected. The most active axis is in the y direction mainly because of the orientation in which the sensor is mounted onto the leg. Figure 3.8 is a similar analysis of the MotionFit data. This represents data from a participant during the walking set.

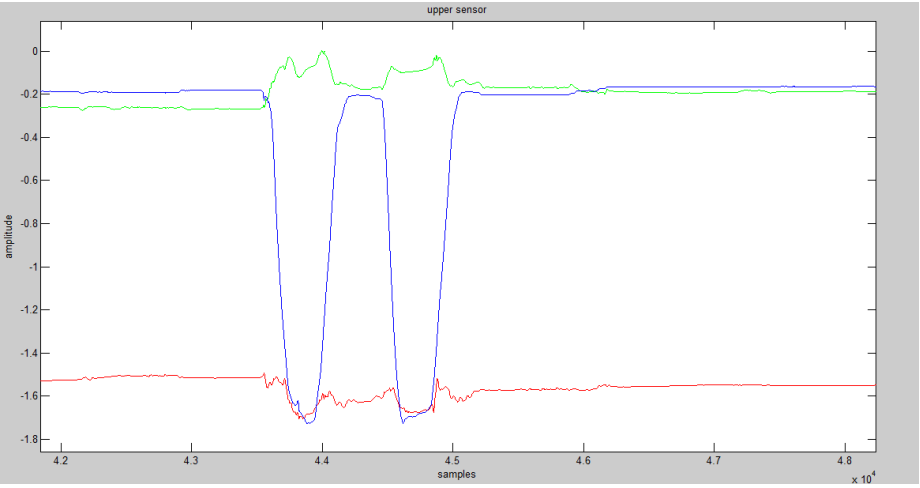

Figure 3.6: Upper sensor data for sit-stand-sit set

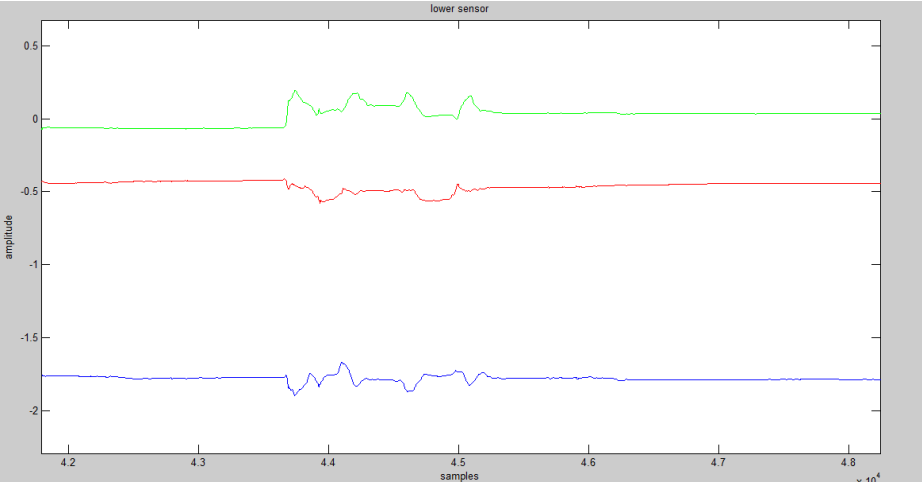

Figure 3.7: Lower sensor data for sit-stand-sit set

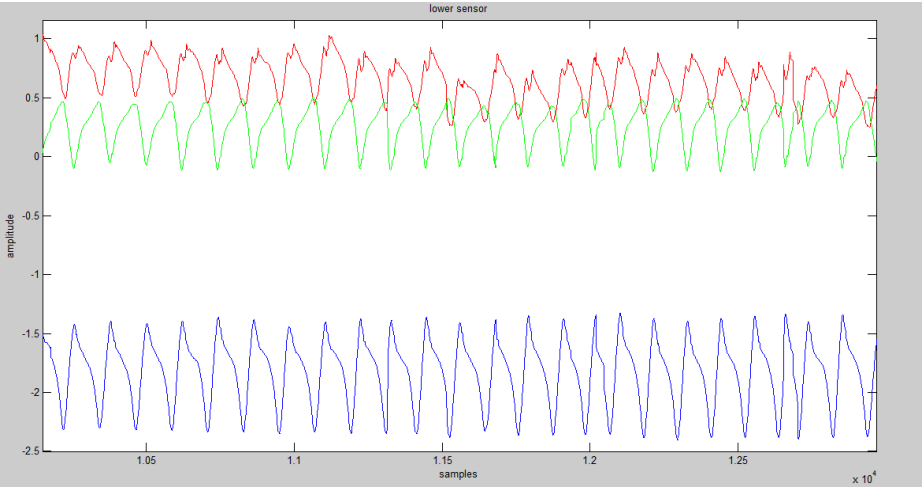

Figure 3.8: Lower sensor data for walking set

An interesting note here is the consistency of the walking movement, which can be an indicator of the nature of the participant's gait. The wave characteristics from a healthy participant can be used as a template for a normal walk, which might imply some level of normalcy for the knee. Figure 3.9 is the processed data from the upper sensor on the same participant. Since the upper leg has less swing in the z and x direction, the periodic waves of these axes have smaller amplitudes. Once we have the movement from both sensors, the angle between the two sensors can be calculated. Using the method described in the previous chapter, the Euler angles of the

knee joint motion are obtained. Figure 3.10 is the joint angle versus the data sample. This represents a sit-stand-sit movement. As expected, the angle of the joint starts close to 90 degrees, approaches 180 degrees, and returns to a right angle. This information, along with video capture of the participant during the movement sets gives us in-depth monitoring capabilities. The acoustic emission can be associated with a movement and time of activity.

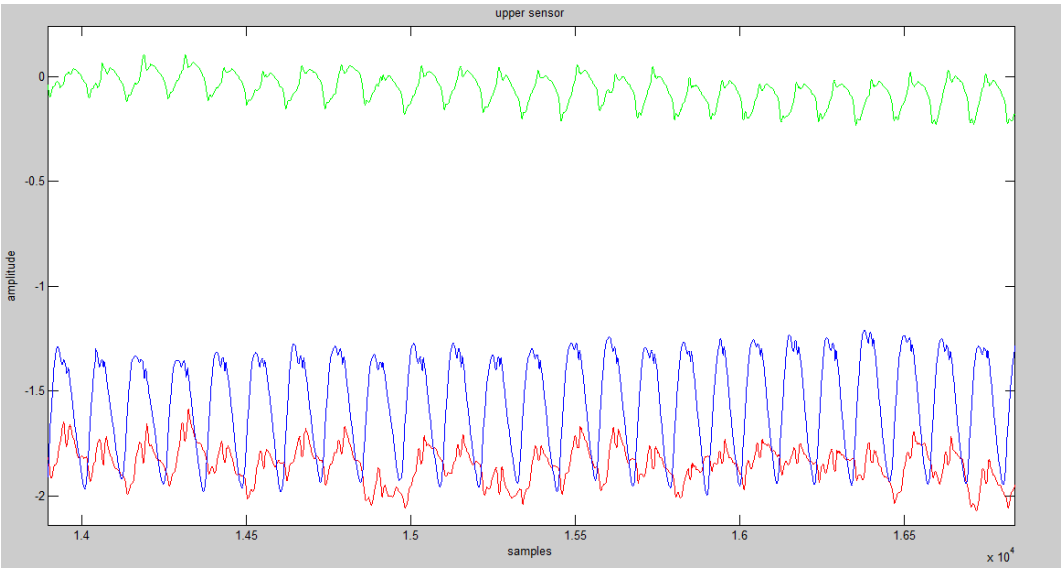

Figure 3.9: Upper sensor data for walking set

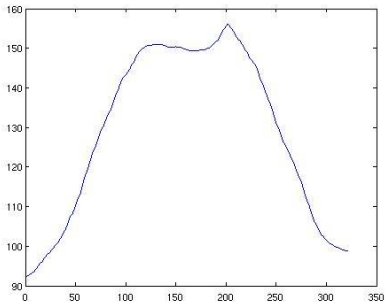

Figure 3.10: Joint angle motion

3.2.2 Acoustic Emission Results

As described in the system design software section of the pervious chapter, AE data acquisition occurs in the triggered mode. The non-continuous recording allows for only the needed data to be saved once waveform characteristics satisfy our defined parameter. Standard deviation is the chosen calculated threshold to which the events are compared. Figure 3.11 is acoustic emissions collected continuously from two sit-stand-sit motions. This was collected from an external data acquisition device and is presented here for reference.

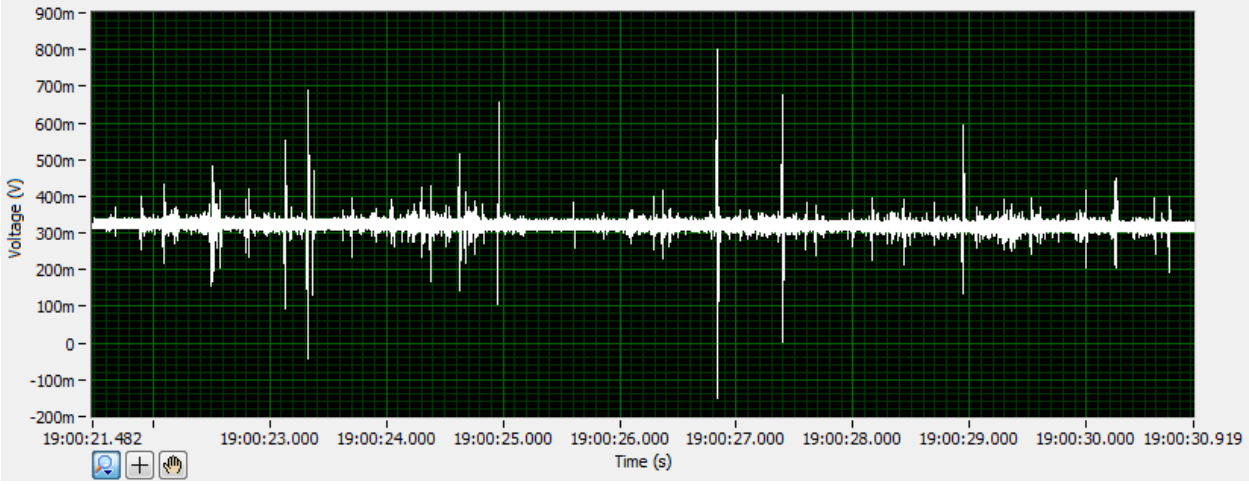

Figure 3.11: Continuous acoustic emissions from sit-stand-sit

The results from the trials have allowed us to collect reoccurring characteristic waves. Figure 3.12 represents a set of waves that are generated from the sensor to skin interface. These events occur when the sensor collects data from the environment (i.e. the knee strap, skin) rather than the AE events from the knee joint. The characteristic features of these waves are their smooth envelope and frequency of about 100MHz. The peak-to-peak amplitude ranges from 200-300mV. Figure 3.13 shows four waves that have inconsistent envelopes and varying frequencies. Higher frequency waves are superimposed on top of the low frequency waves previously discussed.

a)

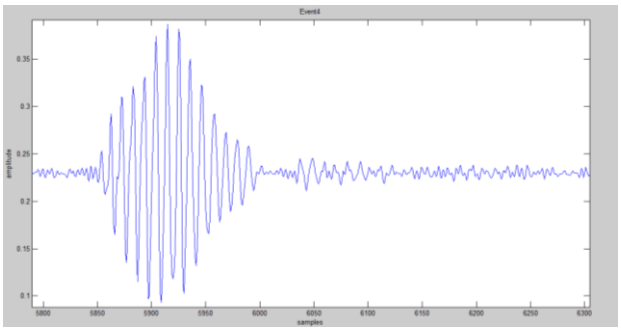

b)

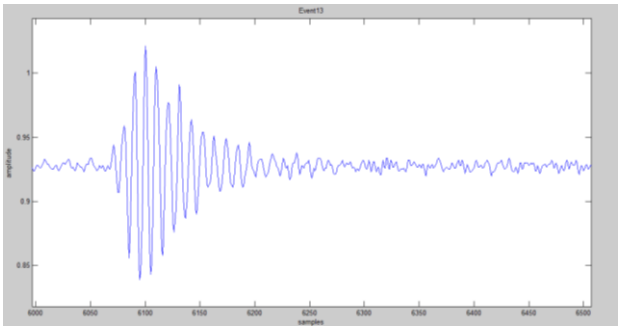

c)

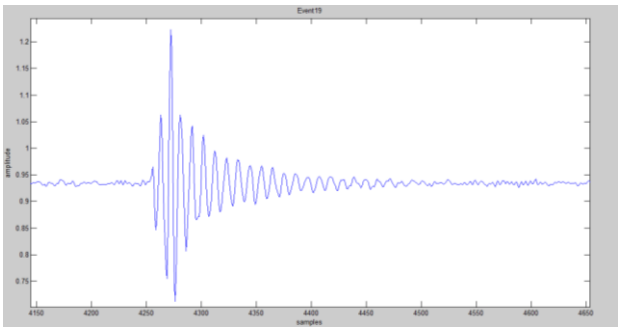

Figure 3.12: AE events from sensor to skin interface

a)

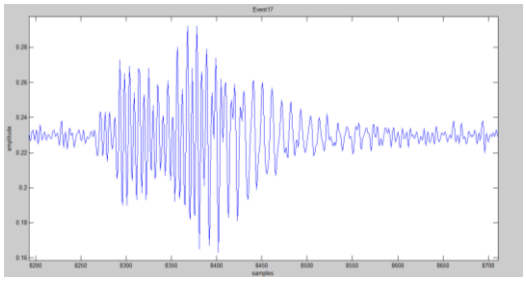

b)

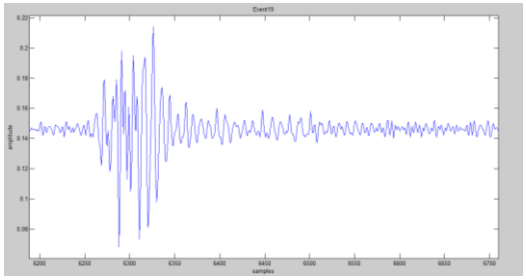

c)

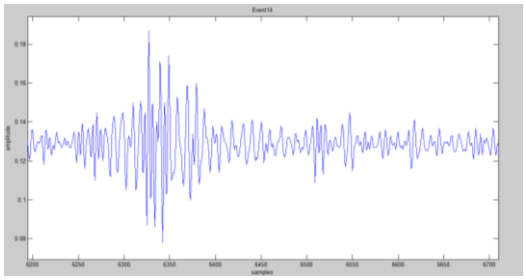

d)

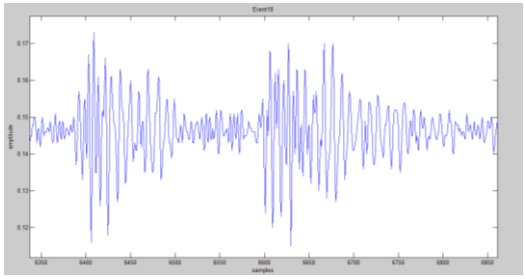

e)

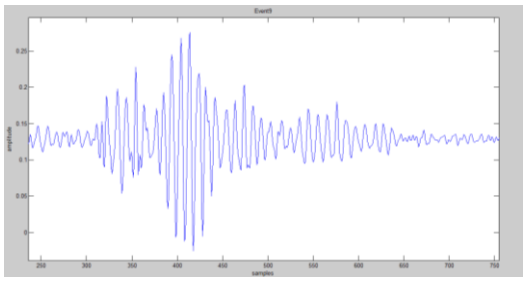

Figure 3.13: Mixed AE events from knee joints

These events are collected from multiple participants and the ones presented here are only a very small fraction of similar waveform captured. The multiple reoccurrences of waves of such nature, along with their timing and frequency, validate the origin of the emissions. The higher frequency characteristics are attributed to AE events from the knee joints. Figure 3.14 demonstrates a set of AE events slightly different in their main features.

a)

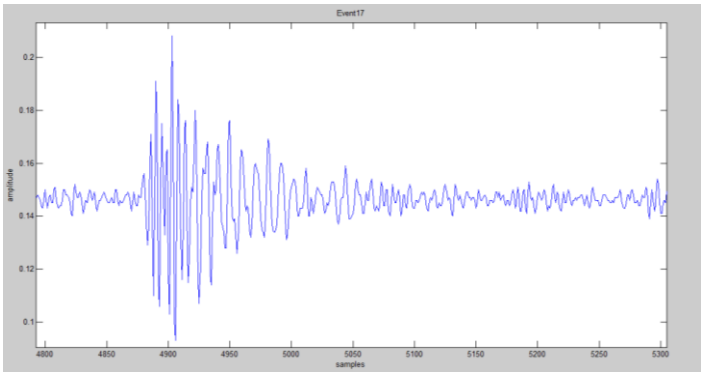

b)

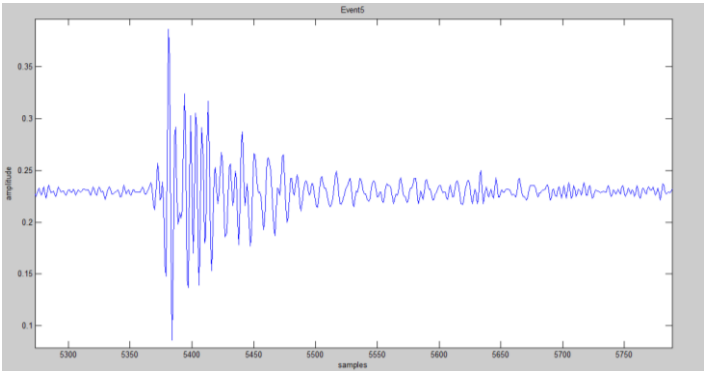

c)

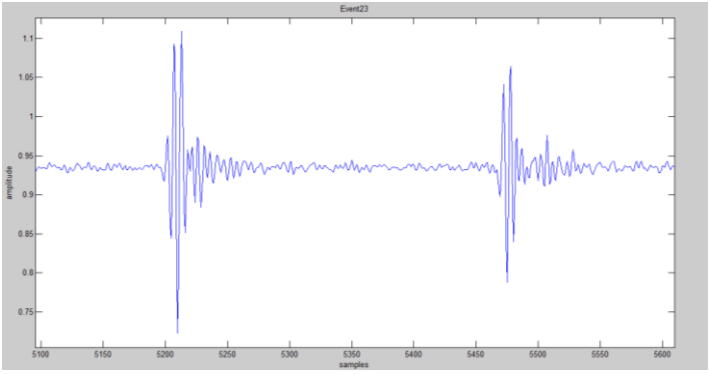

Figure 3.14: AE events from knee joints

a)

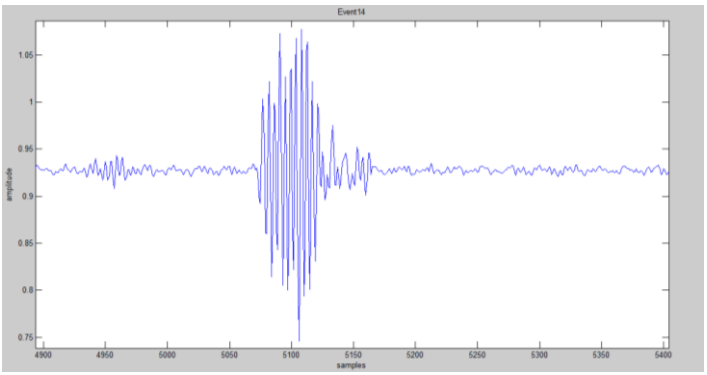

b)

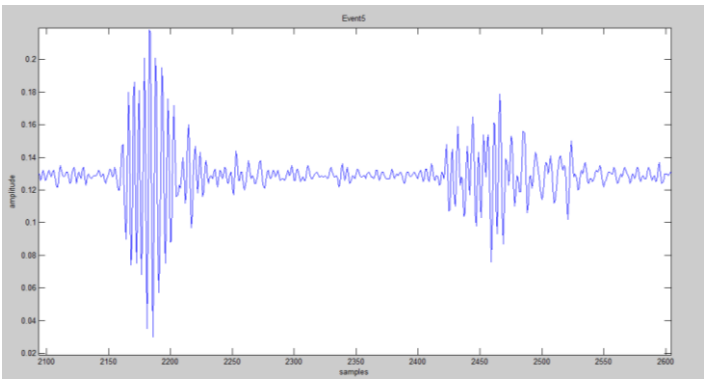

c)

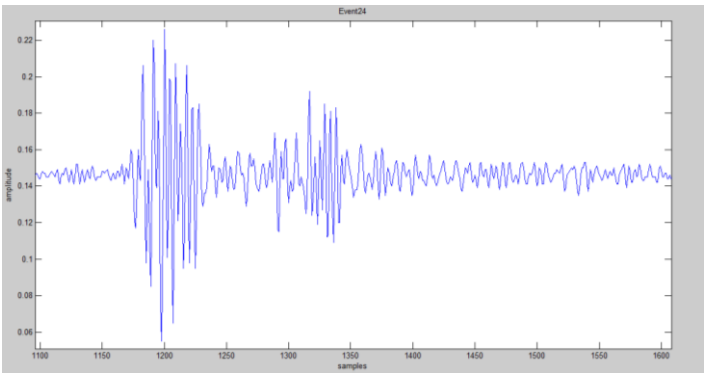

Figure 3.15: Short AE events from knee joints

Unlike the previous, these waves have more predictable envelopes which have a fast rise and a slower fall. However, they are still superposition of low (100Hz) and high frequencies. Figure 3.15 represents the last set of AE events. Here, the high frequency waves are stand-alone and have a unique diamond envelope shape. The occurrences of these events are much less frequent in the healthy participants and do not appear in the older healthy knee participants.

Figures 3.16, 3.17 and 3.18 show the entirety of the information the system provides. The blue underlying line is the knee joint angle provided from the JAM system and the post-processing calculations. The red vertical lines are the AE events plotted according to the time they were captured. The two data sets are synchronized to show the relationship between the motion of the knee during a sit-stand-sit, for example, and the acoustic emission occurring during the movement. From Figure 3.16 it can be noted that the AE events are more spread out in time during the descent of the sit-stand-sit. From Figure 3.17 it can be seen that the number of total AE events is much higher than in a younger healthy knee. Figure 3.18 is a slightly different representation of a similar set of data.

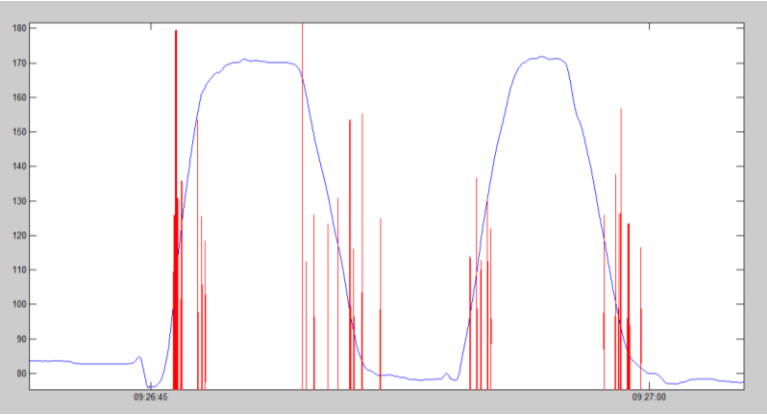

Figure 3.16: AE and JAM from younger knee

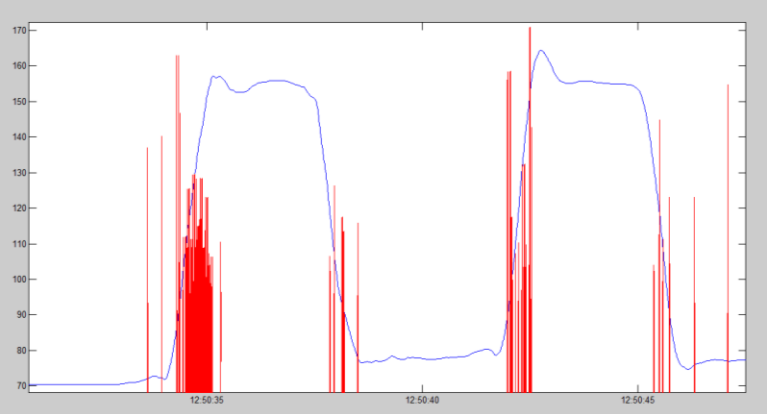

Figure 3.17: AE and JAM from older knee

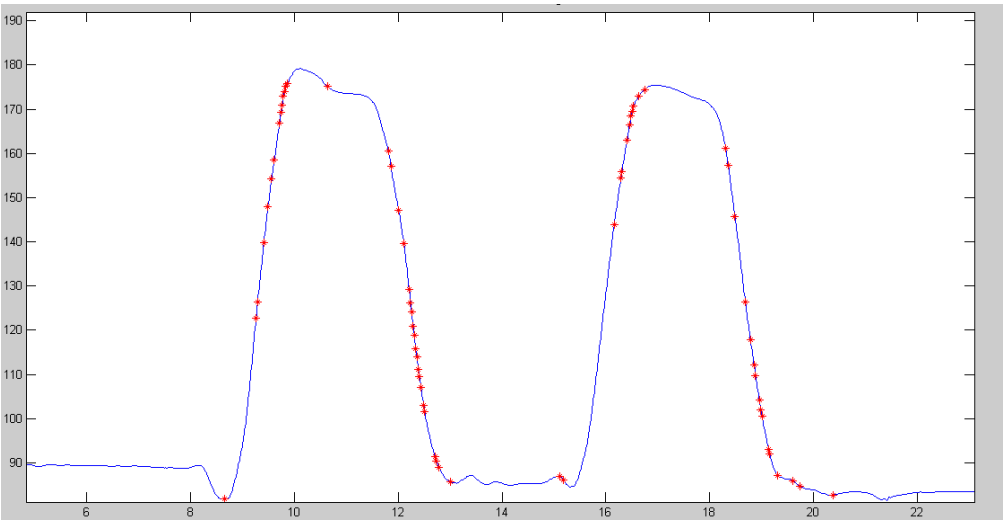

Figure 3.18: AE and JAM results superimposed

Chapter 4

Conclusion and Future Work

With the work we presented here, we aspire to bring forth a new wave of wireless health technologies, which allows us to shift our focus from the traditional event-driven healthcare model to a pervasive health monitoring model where we are continuously monitoring a person's well-being. With the need for quicker, better and low cost healthcare, holistic diagnostics becomes essential. With osteoarthritis being the leading cause of disabilities in the United States, early diagnostics and treatment is of very high importance.

The Wireless Health Orthopedics (WHO) system described in this thesis is a platform for monitoring joint health through the integration of acoustic emission and joint angle motion detection. The system’s wireless feature allows a physician to design trials with a great range of

activities. The system is light weight to allow the patient to wear the device with ease. The high speed sampling provides a clear view of the captured events for further analysis and characterization. We have demonstrated the efficacy of the system presenting integrated JAM and AE information. From the healthy subject trial results we have concluded that AE events do have distinct profiles unique to the participant's age. Furthermore, the quantity of events is an indication of joint age.

Future work will include capturing events from other critical joints, such as the hip and elbows, and even prosthetic joints. A more immediate goal will be to decrease the physical footprint of the system. A smaller size would allow the system to be more lightweight and compact. We will also be extending the trials to a greater number of healthy participants performing a larger array of activities. The healthy subject trials will be followed by monitoring patients who suffer from osteoarthritis of the knee. The data collected from these trials will enable a library of acoustic events defined by their unique features and attributes. They will also include the angle of the joints during which each characteristic event was captured. We believe this library will not only be essential for scientific progress, but will also open up a new avenue through which physicians can confidently diagnose and treat patients.

References

[1] *Arthritis: The Nation's Most Common Cause of Disability*. Center for disease control and prevention. 12 April 2012. Web. ‹http://www.cdc.gov/chronicdisease/resources/publications/aag/arthritis.htm.›

[2] G. Peat, R. McCarney, P. Croft. *Knee pain and osteoarthritis in older adults: a review of community burden and current use of primary health care*. Ann Rheum Dis 2001;60:91-97.

[3] W. Zhang, M. Doherty, G. Peat et al. *EULAR evidence-based recommendations for the diagnosis of the knee osteoarthritis.* Ann Rheum Dis 2010; 69(3):483-9.

[4] Schwalbe HJ, Bamfaste G, Franke RP. *Non-destructive and non-invasive observation of friction and wear of human joints and of fracture initiation by acoustic emission*. Proc Inst Mech Eng H 1999;213:41–8.

[5] J. Prior, B. Mascaro, L.-K. Shark, J. Stockdale, J. Selfe, R. Bury, et al. *Analysis of high frequency acoustic emission signals as a new approach for assessing knee osteoarthritis*. Ann Rheum Dis 2010;69(5):929-30.

[6] L.-K. Sharka, H. Chena, J. Goodacreb. *Knee acoustic emission: A potential biomarker for quantitative assessment of joint ageing and degeneration*. Med Eng & Phys 2011; 33:534-545.

[7] R.P. Franke, P. Dörner, H.-J. Schwalbe, B. Ziegler. *Acoustic Emission Measurement System for the Orthopedical Diagnostics of the Human Femur and Knee Joint*. EWGAE 2004; Lecture 1.

[8] *CompactRIO Integrated Systems with Real-Time Controller and Reconfigurable Chassis NI cRIO-907x*. National Insturments, 25 January 2012. Web. ‹http://sine.ni.com/ds/app/doc/p/id/ds-354/lang/en›.

[9] *4-Channel, 1 MS/s/ch C Series Analog Input Modules NI 9222, NI 9223I.* National Insturments, 18 December 2012.Web. ‹http://sine.ni.com/ds/app/doc/p/id/ds-260/lang/en›.

[10] *Wireless Ethernet Bridge (WET54G).* Linksys by Cisco, 2007. Web. ‹http://support.linksys.com/en-us/support/bridges/WET54G›.

[11] *R15α Sensor: General Purpose Sensor.* MISTRAS Group, 2011. Web. ‹http://www.mistrasgroup.com/products/company/publications/2$Acoustic_Emission/Model_R15a.pdf›.

[12] *Voltage Preamplifiers*. Physical Acoustics Corporation, 2010. Web. ‹http://www.pacndt.com/index.aspx?go=products&focus=/amplifiers/voltagepreamps.htm›.

[13] *Micro30D Sensor: Miniature Differential Sensor*. MISTRAS Group, 2011. Web. ‹http://www.mistrasgroup.com/products/company/publications/2$Acoustic_Emission/Model_Micro30D.pdf›.

[14] *TP140C*. Thunder Power RC, 2013. Web. ‹http://thunderpowerrc.com/html/TP1430C.html›.

[15] *Using DMA FIFO to Develop High-Speed Data Acquisition Applications for Reconfigurable I/O Devices*. National Instruments, 3 March 2012. Web. ‹http://www.ni.com/white-paper/4534/en›.

[16] *MPU-9150 Nine-Axis (Gyro + Accelerometer + Compass) MEMS MotionTracking™ Device*. InvenSense, 2013. Web. ‹http://www.invensense.com/mems/gyro/mpu9150.html›.

[17] *Nine-Axis Sensor Fusion Using the Direction Cosine Matrix Algorithm on the MSP430F5xx Family*. Texas Instruments, February 2012. Web. ‹http://www.ti.com/lit/an/slaa518a/slaa518a.pdf›.

[ba18] *Knee Pain Health CenterI*. WebMD, 2010. Web. ‹http://www.webmd.com/pain-management/knee-pain/picture-of-the-knee›.